IEEE Photonics Journal
An IEEE Photonics Society Publication

Open Access

One-Dimensional Silicon Nitride Grating Refractive Index Sensor Suitable for Integration With CMOS Detectors

Volume 9, Number 1, February 2017

Abdul Shakoor
Marco Grande
James Grant
David R. S. Cumming

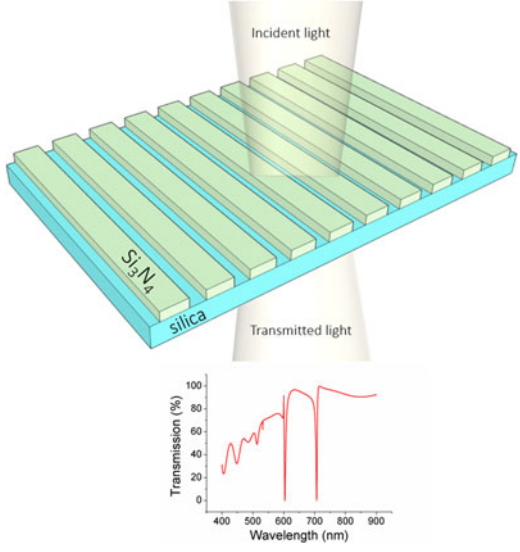

DOI: 10.1109/JPHOT.2016.2644962
1943-0655 © 2016 IEEE

IEEE photonics SOCIETY

IEEE

One-Dimensional Silicon Nitride Grating Refractive Index Sensor Suitable for Integration With CMOS Detectors

Abdul Shakoor,[1] Marco Grande,[2] James Grant,[1] and David R. S. Cumming[1]

[1]School of Engineering, University of Glasgow, Glasgow G12 8LT, U.K.
[2]Dipartimento di Ingegneria Elettrica e dell'Informazione, Politecnico di Bari, Bari 70125, Italy

DOI:10.1109/JPHOT.2016.2644962

Manuscript received November 18, 2016; revised December 15, 2016; accepted December 18, 2016. Date of publication January 9, 2017; date of current version January 12, 2017. This work was supported by the Engineering and Physical Sciences Research Council, U.K., under Grant EP/K021966/1. The work of M. Grande was supported by Fondo di Sviluppo e Coesione 2007–2013–APQ Ricerca Regione Puglia "Programma regionale a sostegno della specializzazione intelligente e della sostenibilità sociale ed ambientale–FutureInResearch" (7K76VI3). Corresponding authors: A. Shakoor and D. R. S. Cumming (e-mail: abdul.shakoor@glasgow.ac.uk; david.cumming.2@glasgow.ac.uk).

Abstract: The transformation of nanophotonic sensors from laboratory-based demonstrations to a portable system to ensure widespread applicability in everyday life requires their integration with detectors for direct electrical read out. As complementary metal oxide semiconductor (CMOS) technology has revolutionized the electronics industry, the integration of nanophotonic structures with CMOS technology will also transform the sensing market. However, nanophotonic sensors have to fulfill certain requirements for their integration with CMOS detectors, such as operation in the visible wavelength range, operation in normal incidence configuration, use of CMOS compatible materials, and capability to give large optical intensity change due to resonance wavelength shift. In this paper, we have designed and developed one-dimensional silicon nitride grating structures that satisfy all these conditions simultaneously. The gratings can achieve 1 and 6 nm linewidths for the transverse-electric (TE) and transverse-magnetic (TM) polarizations, respectively, with 90% resonance depth. The experimental linewidth is 8 nm with 55% resonance depth, which is limited by the detector resolution. The experimental sensitivity of the device is 160 nm/refractive index unit (RIU), which translates to a very high intensity sensitivity of 1700%/RIU, which would enable sensing of very small changes in refractive index when integrated with a detector.

Index Terms: Nanophotonics, diffraction gratings, sensors.

1. Introduction

There is growing interest in developing integrated nanophotonic resonant structures for bio-sensing applications due to their ability to perform quick and label free sensing [1]–[3], high sensitivity [4], [5], and compactness [6], [7] of nanophotonic sensor chips. Nanophotonic sensors are usually based on the phenomenon of refractive index sensing, where a change in the refractive index, induced by the introduction of an analyte or surface binding of bio-species, causes a shift in the resonance wavelength of the nanostructures. Presently, one common drawback among all the nanophotonic based sensors is that their wavelength shift is measured by an external and large

volume optical spectrum analyser which makes their use in everyday life challenging. To make the widespread applicability of nanophotonic sensors possible it is important to integrate them directly with the detector and have a direct electrical readout. Doing so will lead to an easy to use, compact and portable sensing device. For integrating nanophotonic sensors with a detector, photodiodes (PDs) and single photon avalanche diodes (SPADs) made by complementary metal-oxide semiconductor (CMOS) technology are the most suitable choice due to a number of advantages on offer, for example, ease of merging photonic and electronic functionalities, high integration density and lower cost. However, for integration with CMOS technology, there are certain requirements that need to be fulfilled by nanophotonic structures which are listed as follows; (i) their resonance wavelength should be below the bandgap of silicon (1100 nm) where it has high absorption especially in the visible range where the responsivity of the CMOS detector is highest, (ii) the structures should operate in a normal incidence configuration (iii) the material used should be CMOS compatible and (iv) the change in light intensity caused by the resonance wavelength shift must be large. In addition to sensitivity, which is the degree of wavelength shift per refractive index unit (RIU) and the most commonly used Figure of Merit (FOM) for resonant nanophotonic refractive index sensors [8], the change in readout optical intensity due to resonance wavelength shift can also be increased by narrowing the resonance linewidth and increasing the resonance depth, which is the difference in the transmission level between the resonance dip and the highest background transmission level. Hence, not only the sensitivity but the role of resonance linewidth and resonance depth becomes significant for a nanophotonic sensor integrated with a detector.

Photonic nanostructures made of different materials such as metals [9]–[13], dielectrics [14]–[16] or semiconductors [17], [18] and having different design configurations for example waveguide, cavity or grating based devices have been demonstrated for sensing applications, each having its own advantages and shortcomings. While metallic nanostructures such as nanoparticles [19], arrays of nanoholes [20], [21] or nanodiscs [12] and nanoslits [11], [13] achieve high sensitivity by exploiting the plasmonic response, they suffer from high losses which results in a broad resonance linewidth (small Q-factor). On the other hand, dielectric and semiconductor resonant nanostructures such as ring resonators [22], [23], photonic crystal cavities [24], [25] and gratings [26], [27] have higher Q-factors (narrow resonance linewidth) but lower sensitivity compared to plasmonic sensors. Smaller linewidths have an advantage of producing a larger intensity change for a certain degree of wavelength shift. However, a small linewidth results in a smaller dynamic range which is the degree of refractive index change measured by the detector before a change in intensity due to wavelength shift saturates. Therefore, for applications where a large change in refractive index is involved, broadband plasmonic structures will perform better. On the other hand, to improve the detection limit by enabling measurement of very small variations in refractive index, narrow linewidth resonant structures are required.

In this paper, we have designed and developed silicon nitride (Si_3N_4) based 1D grating structures that satisfy all the conditions required for integration with CMOS detectors listed earlier. Although nanophotonic sensors based on different materials and design configurations including grating structures have been demonstrated in the past they do not fulfill all the requirements required for integration with CMOS technology. For example, recently 1-D high contrast gratings made of silicon have been demonstrated for bio-sensing applications but they operate at 1540 nm [27], and being made of silicon they are not suitable for integration with CMOS detectors. To shift the operation range to visible wavelengths silicon nitride based nanophotonics sensors have been demonstrated but they mostly operate in a lateral configuration [14], [15], [28]–[30], which is not useful for integration with CMOS detectors. There are only few reports on silicon nitride based nanophotonic sensors operating in a normal incidence configuration such as sensors based on 2-D photonic crystal membranes [16], [31], but they have a very low degree of robustness since membrane structures are prone to breakage. The 1-D silicon nitride grating structures presented in this report are robust, made of CMOS compatible material, their operation range can be easily tuned in the whole visible to near IR range, operate in a normal incidence configuration and are optimized to give a large change in optical readout intensity due to resonance wavelength shift.

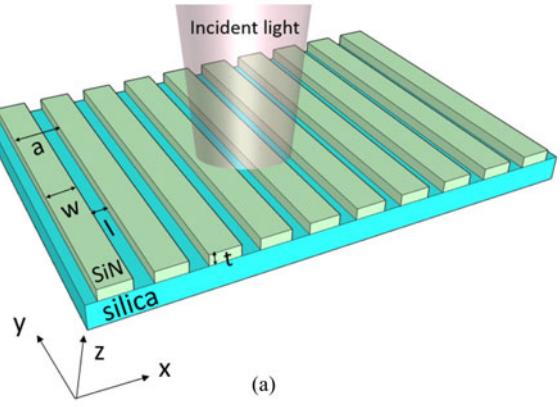

(a)

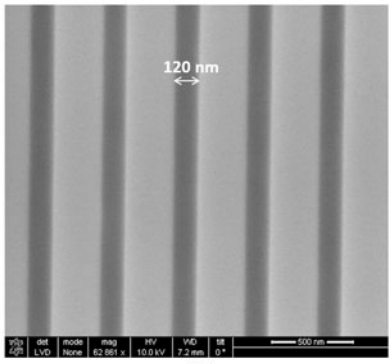

(b)

Fig. 1. (a) Schematic representation of the grating structures: *a*, *w*, and *t* represent the periodicity, width and thickness of gratings, respectively, and *l* represents the airgap. (b) SEM image of the fabricated gratings.

Hence, to the best of our knowledge, this work is the first demonstration of nanophotonic sensors that combine all the characteristics (listed above) required for their integration with CMOS detectors.

2. Grating Design

The 1-D gratings were designed by using the Rigorous Coupled Wave Analysis (RCWA) based commercial software Rsoft (Diffract - MOD). The configuration consists of Si_3N_4 gratings (refractive index, $n_{Si3N4} = 2$) on a borosilicate glass substrate ($n_{sub} = 1.5$) and having either air or liquid as an upper cladding, as shown in the schematic representation in Fig. 1(a), where *a*, *t*, and *w* is periodicity, thickness and width of gratings, respectively, and *l* is the width of the air gap. These gratings support Guided Mode Resonances (GMRs) and can be defined as waveguide-grating resonance structures [32]. A guided mode can be excited only if the effective waveguide refractive index of the i-th order mode Ni (β_i/k_0) satisfies the following inequality:

$$\max\left\{n_{sub}, n_{up}\right\} \leq |N_i| \leq n_{avg} \tag{1}$$

where n_{sub}, n_{up} are the substrate and upper cladding (air or liquid) refractive indices, respectively while n_{avg} is the average refractive index of the grating structures, $k_0 = 2\pi/\lambda_0$ (λ_0 is the free-space wavelength) and β_i is the propagation constant of the *i*-th order mode [32]. Applying the phase-matching condition, (1) can be written as follows:

$$max\left\{n_{sub}, n_{up}\right\} \leq \left|n_{up} sin\theta_{inc} - i\frac{\lambda_0}{a}\right| \leq n_{avg} \tag{2}$$

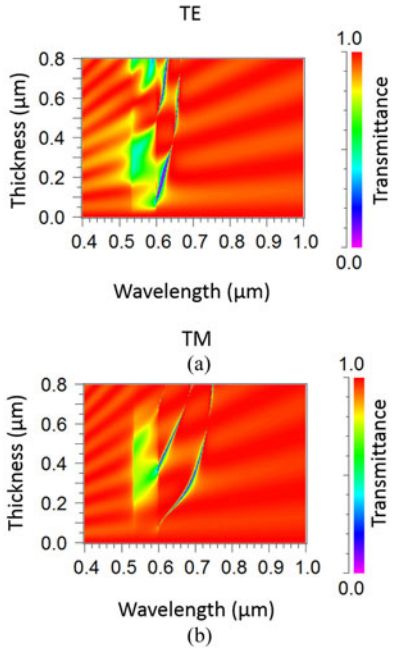

Fig. 2. Simulated transmission maps for different slab thicknesses while keeping the periodicity and fill factor fixed at 400 nm and 0.7, respectively, and having water as an upper cladding for (a) TE and (b) TM polarizations. Note that the resolution used in simulations is kept at 1 nm to match the resolution limit of our measurement setup.

where θ_{inc} is the incident angle and a is the grating periodicity. For normal incidence ($\theta_{inc} = 0$), (2) reduces to the following expression:

$$\max\left\{n_{sub}, n_{up}\right\} \leq \left|i\frac{\lambda_0}{a}\right| \leq n_{avg}. \tag{3}$$

In our device configuration, n_{sub} is always higher than n_{up} (air or liquid), and hence, the minimum operating wavelength $\lambda_{0min} = an_{sub}$. In order to set the first resonance in the visible range, we fixed $\lambda_{0\text{min}} = 600$ nm, the wavelength around which the responsivity of the CMOS detector is high, which leads to the grating periodicity (*a)* of 400 nm. Finally, we set the fill factor (FF $= w/a$) equal to 0.7. A higher fill factor (i.e. smaller air gaps) gives narrower resonance linewidths. However, gratings with narrow air gaps are difficult to fabricate due to their high aspect-ratio. Hence, the choice of fill factor was predominantly based on the fabrication limitations.

Keeping the periodicity and fill factor fixed at 400 nm and 0.7, respectively, the thickness of gratings was optimized to achieve a dual resonance response, one in the visible and a second in the near infrared (IR) region so that the same device can be used for sensing experiments where the required incident wavelength can range from the visible to near IR. Fig. 2(a) and (b) show the simulated transmittance maps of the gratings having water as an upper cladding for the transverse electric (plane of incidence *x-z* and electric field along y, TE) and transverse magnetic (plane of incidence *x-z* and magnetic field along y, TM) polarizations, respectively for different grating thicknesses, *t*. Fig. 2(a) shows that for the TE polarization, there is only one sharp resonance when *t* is lower than 550 nm. As can be seen from Fig. 2(a), Fabry–Pérot fringes interfere with the resonance. Due to the modulation of the resonance by the interference of the Fabry–Pérot fringes, the second resonance response is not as sharp as the first resonance. The second resonance becomes sharper by increasing the silicon nitride thickness to at least 550 nm however fabricating such high aspect ratio structures is challenging.

On the contrary, for TM polarization, two sharp resonances, one in the visible and other in the near infrared (near IR) region appears at thickness of 350 nm and above, as shown in Fig. 2(b).

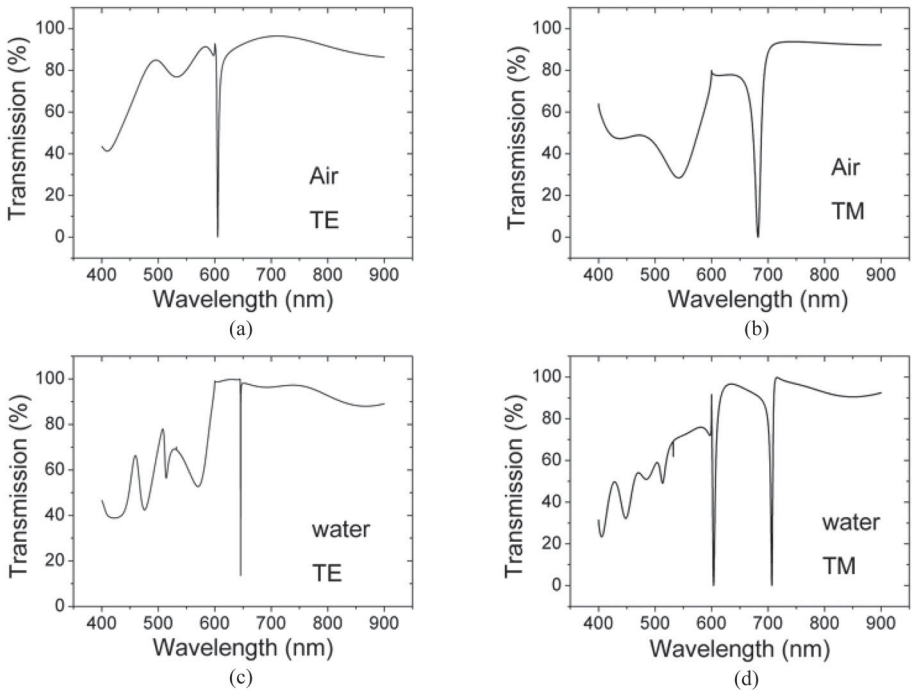

Fig. 3. Simulated transmission spectra of the grating structures having the following physical parameters, t = 400 nm, a = 400 nm, l = 120 nm, and w = 280 nm. (a) TE polarization, air cladding. (b) TM polarization, air cladding. (c) TE Polarization, water cladding. (d) TM polarization, water cladding. As in Fig. 2(a) and (b), the resolution used for simulating transmission spectra is also kept as 1 nm.

Therefore, we fixed the grating thickness at 400 nm which gives two narrow linewidth resonant transmission responses having a high resonance depth to achieve a large change in optical readout intensity for a certain degree of wavelength shift.

The simulated transmission spectra for the optimized physical grating parameters i.e., a = 400 nm, t = 400 nm, and FF = 0.7, are given in Fig. 3, which show a resonance linewidth of 2 nm and 15 nm for TE and TM polarizations respectively (for air cladding) with 90% resonance depth.

The resonance linewidth reduces to 1 nm and 6 nm for TE and TM polarizations respectively when a higher refractive index upper cladding such as water is used, as evident by comparing Fig. 3(a) with (c) and Fig. 3(b) with (d). Conversely, the resonance depth does not change. In the simulation results shown in Fig. 3(c) and (d), it is assumed that the water fills the grooves. We also carried out simulations for the case where water penetrates only half of the air slot with lower half filled with air, which did not show any significant change in the mode profile or the sensitivity of the grating structures. Similar trends were observed for gratings with 450 nm periodicity having resonance responses at higher wavelengths. Hence, by using different periodicities the operating range of the device can be tuned easily.

3. Methods

3.1. Fabrication

The grating structures were fabricated by a standard e-beam lithography process followed by reactive ion etching using an e-beam resist ZEP 520A as an etch mask. First, a 400 nm thick Si_3N_4 layer was deposited on top of a 500 μm thick borosilicate glass substrate using a plasma enhanced chemical vapour deposition (PECVD) process. Afterwards a 250 nm thick layer of ZEP 520A dissolved in anisole (2:1 ratio) was deposited on top of the Si_3N_4 layer by spin coating.

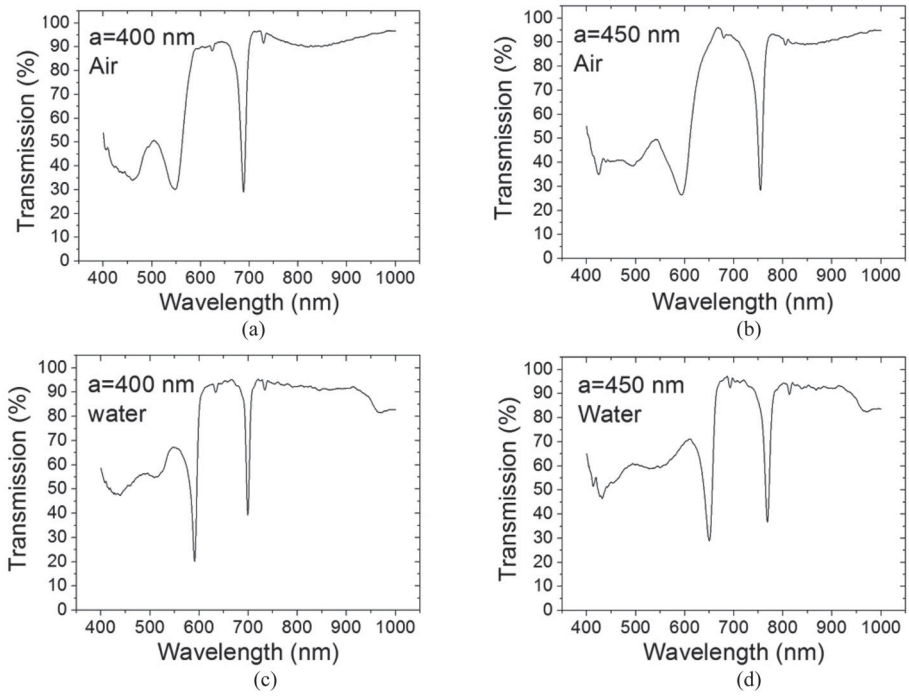

Fig. 4. Measured transmission spectra of the grating structures for TM polarization. (a) 400 nm period with air cladding. (b) 450 nm period with air cladding. (c) 400 nm period with water cladding. (d) 450 nm period with water cladding.

The grating structures were defined in the resist by e-beam exposure followed by resist development by o-xylene. The grating patterns were transferred to Si_3N_4 layer by reactive ion etching using a CHF_3/O_2 gas chemistry. After etching, the e-beam resist was removed using 1165 remover. The physical dimensions of the fabricated grating structures were measured using a scanning electron microscope (SEM). An SEM image of the fabricated gratings is shown in Fig. 1(b).

3.2. Characterization

The transmission response of the device was measured using a commercial Foster and Freeman microspectrometer attached to a DM2700M Leica microscope. A halogen lamp was used as the incident light source and the grating structures were illuminated in normal incidence condition. The light transmitted through the grating structures was collected by a 4x objective having a numerical aperture of 0.1. The collected light was polarized and fed to a spectrometer via an optical fiber which gives the transmission spectrum of the grating structures. To carry out experiments with an aqueous cladding, an encapsulated ring was attached around the gratings to contain the liquid on top of the structures.

4. Experimental Results and Discussion

From the simulation results discussed in Section 2, it is found that for TE polarization at $t = 400$ nm, a single very sharp resonant transmission response is present having a bandwidth of around 1 nm which is the resolution limit of our measurement setup and hence the transmission response for TE polarization could not be measured. Furthermore, as these grating structures are optimized for their future integration with CMOS detectors to remove the requirement of large and expensive laboratory based equipment such as an optical spectrum analyser and laser, the use of very narrow line width structures ($<$5 nm, as is the case with TE polarization) is not practical as it would require a laser

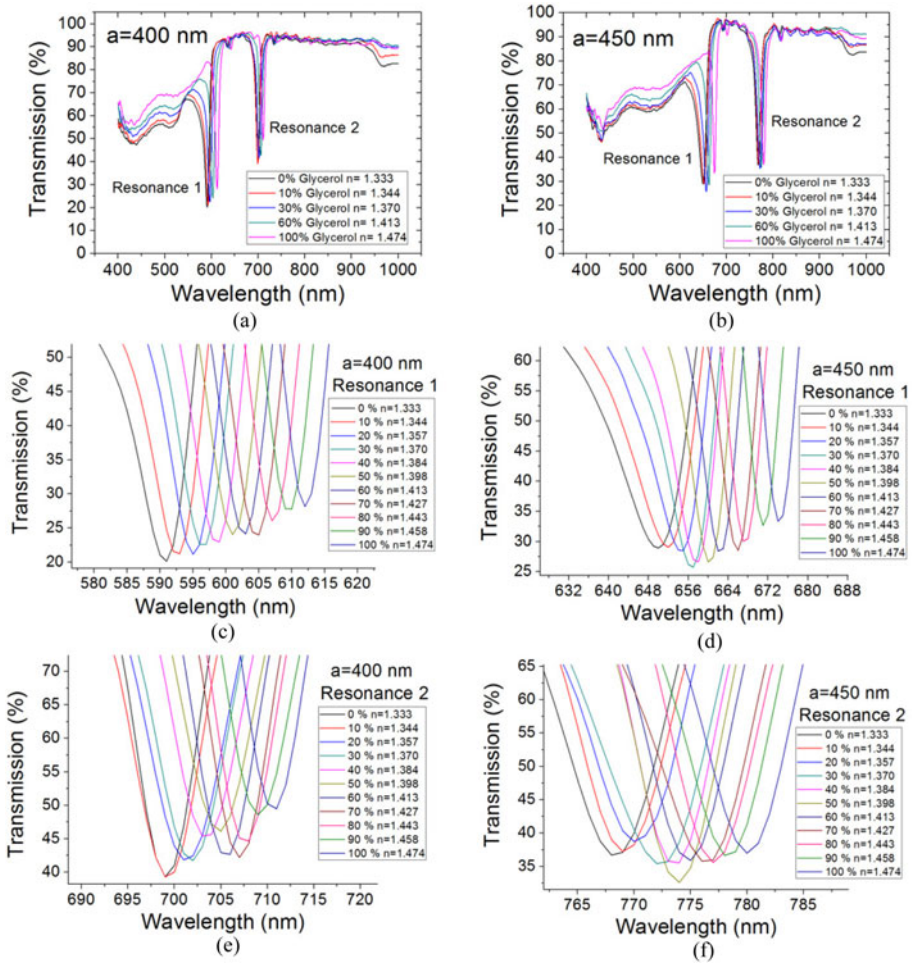

Fig. 5. Experimental resonance wavelength shift due to increase in refractive index of the cladding layer corresponding to different concentrations of glycerol for grating periods (a) 400 nm and (b) 450 nm. Only selected curves are shown for the purpose of clarity. (c), (e) Zoomed in presentation of two resonances for a grating period 400 nm and (d), (f) a grating period of 450 nm showing the change of concentration in smaller steps.

with a comparable or narrower linewidth as the input light source. Hence grating structures with a resonance linewidth around 10 nm are more suitable as it will allow the use of a light emitting diode (LED) as an input light source. For this reason, we shall consider only TM polarization hereafter. The measured transmission responses of the grating structures for TM polarization with air and water cladding layers for two different periods (400 and 450 nm) are shown in Fig. 4. The transmission responses are normalized to the transmission through an identical glass substrate in air on top of which grating structures are fabricated. The linewidths and transmission minima wavelength positions match very well with the simulation results shown in Fig. 3. However, the measured resonance depth is lower compared to simulations due to limitations of the detector resolution. For air cladding, the measured transmission dip at longer wavelength has a linewidth of 15 nm and a resonance depth of 65%, which reduces to 8 nm and 55%, respectively, for water cladding. While the linewidth narrowing is due to higher refractive index cladding, the reduction in resonance depth is because of the limitation of the detector resolution. Similar to the response in the near IR, the transmission linewidth in the visible range also gets narrower by adding liquid as a cladding layer, which is also supported by the simulations.

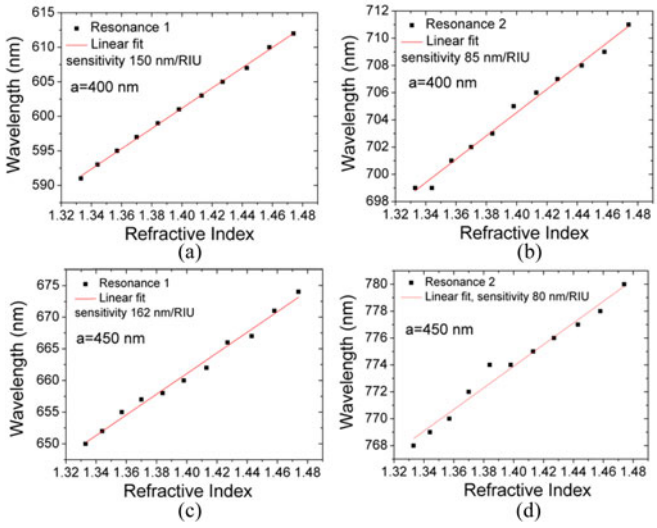

Fig. 6. Experimental resonance wavelengths for different refractive indices of the upper cladding. (a) Grating period 400 nm, resonance 1. (b) Grating period 400 nm, resonance 2. (c) Grating period 450 nm, resonance 1. (d) Grating period 450 nm, resonance 2. The slope gives the sensitivity of the device, which is around 160 nm /RIU and 80 nm/RIU for resonances in the visible and near IR, respectively.

The performance of fabricated 1-D Si_3N_4 gratings as a refractive index sensor was evaluated by measuring its transmission response for changes in refractive index of the upper cladding. The refractive index of the cladding was changed systematically by introducing different concentrations of glycerol (weight/weight %) in DI water. The refractive index increases with increasing glycerol concentrations [33]. The transmission spectra of the grating structures for two different periods (400 nm and 450 nm) when different concentrations of glycerol are applied as a cladding layer are given in Fig. 5 and show a red shift of both resonant transmission lines (visible and near IR) for higher concentrations.

The resonance wavelengths at different refractive indices corresponding to different concentrations of glycerol are plotted in Fig. 6, whose gradient gives the device sensitivity. The change in wavelength is linear for both transmission lines, however, for both periods, the experimental sensitivity in the visible range is almost twice (160 nm/RIU) compared to in the near IR (80 nm/RIU).

The analytes used in the experiments (water and glycerol) have negligible extinction coefficient ($k \approx 0$) and, hence, are transparent in the wavelength of interest. Thus, the absorption induced by introducing different concentrations of glycerol in these experiments is negligible. This was also confirmed by carrying out transmission measurements (data not shown here) for different concentrations of glycerol on top of a glass substrate where no changes in the transmission levels was observed proving that the effect of absorption in these experiments is negligible.

As discussed earlier, on integration of nanophotonic sensors with detectors, it is the change in read-out optical signal intensity due to resonance wavelength shift which is important rather than only the wavelength shift itself. Hence, we carried out analysis of the change in transmission level which corresponds to intensity change when different concentrations of glycerol are applied on top of grating structures for different excitation wavelengths. The excitation wavelengths were selected to achieve the maximum measurement range. Fig. 7 shows the analysis of transmission change for the resonant transmission line in the visible range for gratings having a periodicity of 400 nm. Similar trend is observed for gratings having 450 nm periodicity in both the visible and near IR spectral region. From Fig. 7, it can be seen that the curves (% change in transmission for change in refractive index) shows almost a linear response. The slight deviation from linearity at higher refractive indices is due to limitations in detector reso-

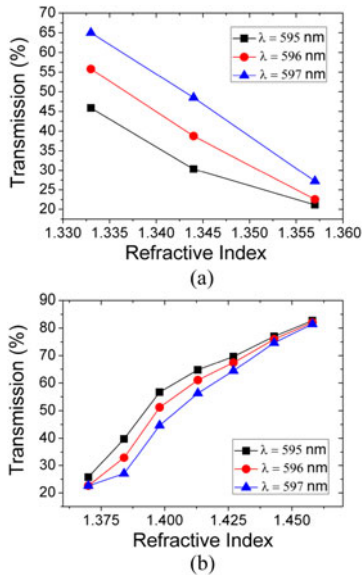

Fig. 7. Experimental change in transmission levels (intensity) due to wavelength shift induced by changing refractive indices by applying different concentrations of glycerol at different excitation wavelengths.

lution, as discussed earlier. For the chosen excitation wavelengths, initially, the transmission levels drop by increasing refractive index values [see Fig. 7(a)] and then increases [see Fig. 7(b)].

The initial decrease in transmission is due to the fact that, until certain refractive index values, the excitation wavelength spectrally overlaps with the leading edge of the transmission dip after which it coincides with the trailing edge which is then measured as an increase in the transmission level. From Fig. 7(a), the sensitivity (in terms of change in intensity per RIU) is estimated to be 1700%/RIU. Similar analysis is also carried out for the resonance in near IR region which gives a sensitivity value of 750%/RIU, almost half of that measured for the resonance in the visible region. This is consistent with the sensitivity responses of both resonances in terms of wavelength shift per RIU, where the sensitivity in the near IR range is also measured to be half compared to the one in the visible range, as shown in Fig. 6. The intensity sensitivity value of 1700%/RIU means that if the detector can measure a 1% change in intensity, then the detection limit of the detector integrated Si_3N_4 grating nanophotonic sensor system will be 5×10^{-4} RIU. The capability to measure such a small change in refractive index will enable the integrated sensor system to easily find applications in bio-sensing where detecting small changes in refractive indices to distinguish bio-species such as protein or DNA is required.

The analysis of change in intensity due to variation of refractive indices shows that even though the sensitivity in terms of wavelength shift (nm/RIU) for these grating structures is not that high (maximum 160 nm/RIU), due to the narrow linewidth and large resonance depth, the sensitivity in terms of change in intensity (ΔI/RIU) is very high (1700%/RIU). Hence, for monolithic integration of nanophotonic structures with detectors to develop a miniaturized and portable nanophotonics sensor with direct electrical read-out, the grating structures presented in this paper are a strong candidate.

5. Conclusion

We have designed and developed 1D Si_3N_4 grating structures that satisfy all the conditions required for future integration of resonant nanophotonic structures with CMOS detectors such as operation below the silicon bandgap (1100 nm), working at normal incidence, material compatibility, and high sensitivity in terms of change in intensity per RIU. By finding the optimum balance between narrow resonance linewidth and a high resonance depth, our grating structures achieve a very

high intensity sensitivity of 1700%/RIU. Furthermore, the grating structures show a dual resonance response, one in the visible and other in the near IR range which enables sensing experiments in both the visible and near IR wavelength ranges. Successful integration of these Si_3N_4 gratings with CMOS detectors would lead to a practical, portable, and handheld nanophotonic sensor system with applications in numerous areas, especially in point-of-care diagnostics.

Acknowledgment

The authors would like to thank technical staff of James Watt Nanofabrication Center, University of Glasgow, for their assistance in device fabrication. The data set for this work can be accessed by following DOI: 10.5525/gla.researchdata.370.

References

[1] A. L. Washburn, M. S. Luchansky, A. L. Bowman, and R. C. Bailey, "Quntitative, label-free detection of five protein biomarkers using multiplexed arrays of silicon photonic microring resonators," *Anal. Chem.*, vol. 82, no. 1, pp. 69–72, 2010.
[2] A. L. Washburn, L. C. Gunn, and R. C. Bailey, "Label-free quantitation of a cancer biomarker in complex media using silicon photonic microring resonators," *Anal. Chem.*, vol. 81, no. 22, pp. 9499–9506, 2009.
[3] X. Fan, I. M. White, S. I. Shopova, H. Zhu, J. D. Suter, and Y. Sun, "Sensitive optical biosensors for unlabeled targets: A review," *Anal. Chim. Acta*, vol. 620, nos. 1–2, pp. 8–26, 2008.
[4] J. Lee, B. Kim, B. Oh, and J. Choi, "Highly sensitive localized surface plasmon resonance immunosensor for label-free detection of HIV-1," *Nanomed. Nanotechnol., Biol. Med.*, vol. 9, no. 7, pp. 1018–1026, 2013.
[5] M. Sumetsky, R. S. Windeler, Y. Dulashko, and X. Fan, "Optical liquid ring resonator sensor," *Opt. Exp.*, vol. 15, no. 22, 2007, Art. ID. 14376.
[6] E. Chow, A. Grot, L. W. Mirkarimi, M. Sigalas, and G. Girolami, "Ultracompact biochemical sensor built with two-dimensional photonic crystal microcavity," *Opt. Lett.*, vol. 29, no. 10, pp. 1093–1095, 2004.
[7] D. Y. Fedyanin and Y. V. Stebunov, "All-nanophotonic NEMS biosensor on a chip," *Sci. Rep.*, vol. 5, 2015, Art. ID. 10968.
[8] I. M. White and X. Fan, "On the performance quantification of resonant refractive index sensors," *Opt. Exp.*, vol. 16, no. 2, pp. 1020–1028, 2008.
[9] J. N. Anker, W. P. Hall, O. Lyandres, N. C. Shah, J. Zhao, and R. P. Van Duyne, "Biosensing with plasmonic nanosensors," *Nature Mater.*, vol. 7, no. 6, pp. 442–453, 2008.
[10] R. Gordon, D. Sinton, K. L. Kavanagh, and A. G. Brolo, "A new generation of sensors based on extraordinary optical transmission," *Accounts Chem. Res.*, vol. 41, no. 8, pp. 1049–1057, 2008.
[11] K.-L. Lee, J.-B. Huang, J.-W. Chang, S.-H. Wu, and P.-K. Wei, "Ultrasensitive biosensors using enhanced Fano resonances in capped gold nanoslit arrays," *Sci. Rep.*, vol. 5, 2015, Art. ID. 8547.
[12] J. A. Ruemmele, W. P. Hall, L. K. Ruvuna, and R. P. Van Duyne, "A localized surface plasmon resonance imaging instrument for multiplexed biosensing," *Anal. Chem.*, vol. 85, no. 9, pp. 4560–4566, May 2013.
[13] B. Zeng, Y. Gao, and F. J. Bartoli, "Rapid and highly sensitive detection using Fano resonances in ultrathin plasmonic nanogratings," *Appl. Phys. Lett.*, vol. 105, no. 16, 2014, Art. ID. 161106.
[14] J. Wang, Z. Yao, and A. W. Poon, "Silicon-nitride-based integrated optofluidic biochemical sensors using a coupled-resonator optical waveguide," *Front. Mater.*, vol. 2, pp. 1–13, 2015.
[15] P. Muellner, E. Melnik, G. Koppitsch, J. Kraft, F. Schrank, and R. Hainberger, "CMOS-compatible Si_3N_4 waveguides for optical biosensing," *Procedia Eng.*, vol. 120, pp. 578–581, 2015.
[16] D. Zecca *et al.*, "Label-free Si_3N_4 photonic crystal based immunosensors for diagnostic applications," *IEEE Photon. J.*, vol. 6, no. 6, Dec. 2014, Art. ID. 0600507.
[17] B. Momeni, S. Yegnanarayanan, M. Soltani, A. A. Eftekhar, E. S. Hosseini, and A. Adibi, "Silicon nanophotonic devices for integrated lab-on-a-chip sensing," in *Proc. Annu. Int. Conf. IEEE Eng. Med. Biol. Soc.*, vol. 3, 2010, pp. 4419–4422.
[18] D. F. Dorfner, T. Hürlimann, T. Zabel, L. H. Frandsen, G. Abstreiter, and J. J. Finley, "Silicon photonic crystal nanostructures for refractive index sensing," *Appl. Phys. Lett.*, vol. 93, no. 18, pp. 2006–2009, 2008.
[19] M. Sriram, K. Zong, S. R. C. Vivekchand, and J. Justin Gooding, "Single nanoparticle plasmonic sensors," *Sensors*, vol. 15, no. 10, pp. 25774–25792, 2015.
[20] A. G. Brolo, R. Gordon, B. Leathem, and K. L. Kavanagh, "Surface plasmon sensor based on the enhanced light transmission through arrays of nanoholes in gold films," *Langmuir*, vol. 20, no. 17, pp. 4813–4815, 2004.
[21] A. De Leebeeck, L. K. S. Kumar, V. de Lange, D. Sinton, R. Gordon, and A. G. Brolo, "On-chip surface-based detection with nanohole arrays," *Anal. Chem.*, vol. 79, no. 11, pp. 4094–4100, Jun. 2007.
[22] Y. Sun and X. Fan, "Optical ring resonators for biochemical and chemical sensing," *Anal. Bioanal. Chem.*, vol. 399, no. 1, pp. 205–211, 2011.
[23] A. Ksendzov and Y. Lin, "Integrated optics ring-resonator sensors for protein detection," *Opt. Lett.*, vol. 30, no. 24, pp. 3344–3346, 2005.
[24] A. Di Falco, L. O'Faolain, and T. F. Krauss, "Chemical sensing in slotted photonic crystal heterostructure cavities," *Appl. Phys. Lett.*, vol. 94, no. 6, pp. 93–96, 2009.

[25] M. G. Scullion, A. Di Falco, and T. F. Krauss, "Slotted photonic crystal cavities with integrated microfluidics for biosensing applications," *Biosens. Bioelectron.*, vol. 27, no. 1, pp. 101–105, 2011.
[26] J. H. Schmid *et al.*, "Silicon-on-insulator guided mode resonant grating for evanescent field molecular sensing," *Opt. Exp.*, vol. 17, no. 20, pp. 18371–18380, 2009.
[27] T. Sun, S. Kan, G. Marriott, and C. Chang-Hasnain, "High-contrast grating resonators for label-free detection of disease biomarkers," *Sci. Rep.*, vol. 6, 2016, Art. ID. 27482.
[28] Q. Liu *et al.*, "Highly sensitive Mach–Zehnder interferometer biosensor based on silicon nitride slot waveguide," *Sens. Actuators, B Chem.*, vol. 188, pp. 681–688, 2013.
[29] E. Melnik *et al.*, "Local functionalization of CMOS-compatible Si_3N_4 Mach–Zehnder interferometers with printable functional polymers," *Sens. Actuators B Chem.*, vol. 236, pp. 1061–1068, 2016.
[30] X. Tu *et al.*, "Thermal independent silicon-nitride slot waveguide biosensor with high sensitivity," *Opt. Exp.*, vol. 20, no. 3, pp. 2640–2648, 2012.
[31] K. Deasy *et al.*, "A chemical sensor based on a photonic-crystal L3 nanocavity defined in a silicon-nitride membrane," *J. Mater. Chem. C*, vol. 2, no. 41, pp. 8700–8706, 2014.
[32] S. S. Wang and R. Magnusson, "Theory and applications of guided-mode resonance filters," *Appl. Opt.*, vol. 32, no. 14, pp. 2606–2613, 1993.
[33] L. F. Hoyt, "New table of the refractive index of pure glycerol at 20 °C," *Ind. Eng. Chem.*, vol. 26, no. 3, pp. 329–332, 1934.